QUANTUM TECHNOLOGY

Robust multi-qubit quantum network node with integrated error detection

P.-J. Stas[1]*, Y. Q. Huan[1]*, B. Machielse[1,2]*, E. N. Knall[3], A. Suleymanzade[1], B. Pingault[3,4,5], M. Sutula[1], S. W. Ding[3], C. M. Knaut[1], D. R. Assumpcao[3], Y.-C. Wei[1], M. K. Bhaskar[1,2], R. Riedinger[1,6,7], D. D. Sukachev[1,2], H. Park[1,8], M. Lončar[3], D. S. Levonian[1,2], M. D. Lukin[1]†

Long-distance quantum communication and networking require quantum memory nodes with efficient optical interfaces and long memory times. We report the realization of an integrated two-qubit network node based on silicon-vacancy centers (SiVs) in diamond nanophotonic cavities. Our qubit register consists of the SiV electron spin acting as a communication qubit and the strongly coupled silicon-29 nuclear spin acting as a memory qubit with a quantum memory time exceeding 2 seconds. By using a highly strained SiV, we realize electron-photon entangling gates at temperatures up to 1.5 kelvin and nucleus-photon entangling gates up to 4.3 kelvin. We also demonstrate efficient error detection in nuclear spin–photon gates by using the electron spin as a flag qubit, making this platform a promising candidate for scalable quantum repeaters.

The ability to distribute quantum information over extended distances (*1*, *2*) constitutes an important enabling technology in quantum information science, with applications in quantum key distribution (*3*, *4*), nonlocal sensing (*5*), and distributed quantum computation (*6*, *7*). A key requirement for the realization of such long-distance quantum networking involves the development of quantum repeaters (*8*) to mitigate photonic qubit loss during transmission over extended distances. These require network nodes containing multiple qubits that can collect, store, and process information communicated through photonic channels (*9*). Although theoretical proposals for all-photonic repeater schemes (*10*) potentially circumvent this requirement, they involve efficient sources of large-scale photonic states, which are very challenging to realize.

Color centers in diamond nanophotonic structures (*11*–*14*) have recently emerged as leading candidates for realizing such nodes owing to their long coherence times, high-fidelity single-qubit gates, efficient qubit-photon interfaces, and high experimental repetition rates. The integration of all these features into a single device has led to the demonstration of memory-enhanced quantum communication (*11*) with the silicon-vacancy (SiV) center. Important steps toward quantum networking have been taken by using multi-qubit registers based on nitrogen-vacancy (NV) centers and nearby nuclear spins (*15*), but the low coupling efficiency to photons makes scalability challenging. Although other promising platforms, such as trapped ions (*16*) and neutral atoms (*17*) in optical cavities, achieved efficient coupling to photons, scalable implementation of quantum repeaters requires access to auxiliary memory qubits to perform entanglement swapping, purification, and error detection (*8*, *9*), which thus far has been challenging to achieve in a single setting. For SiVs, the technical complexity associated with the need for operation at dilution refrigerator temperatures [required to avoid phonon-induced dephasing (*18*)] has thus far impeded the prospects for scalability. Here, we address this long-standing challenge by using a highly strained SiV (*18*, *19*) featuring the ^{29}Si isotope, with its nuclear spin (*20*) serving as a deterministic long-lived memory qubit. We demonstrate full control of this integrated two-qubit register at increased temperatures, including selective qubit readout via a phase-based readout method, enabling multiple electron state resets before deterioration of the nuclear spin memory.

The ^{29}SiV in an external magnetic field constitutes a two-qubit system of four spin states with nondegenerate transition frequencies (Fig. 1A). The electron and nuclear spin qubits are coherently controlled by using microwave (MW) and radiofrequency (RF) pulses, respectively, which are delivered through gold coplanar waveguides (Fig. 1B). The SiV is embedded in a nanophotonic cavity (Fig. 1C), which enhances optical transitions to the excited-state manifold at 737 nm (Fig. 1A, wavy arrows) that is used for state readout and spin-photon entanglement. The SiV-cavity system exhibits high-contrast spin-dependent reflection spectra (Fig. 1D) enabled by the strong cavity coupling [cooperativity $C = 1.6$ (*21*)].

[1]Department of Physics, Harvard University, Cambridge, MA 02138, USA. [2]AWS Center for Quantum Networking, Boston, MA 02210, USA. [3]John A. Paulson School of Engineering and Applied Sciences, Harvard University, Cambridge, MA 02138, USA. [4]QuTech, Delft University of Technology, 2600 GA Delft, Netherlands. [5]Kavli Institute of Nanoscience Delft, Delft University of Technology, 2600 GA Delft, Netherlands. [6]Institut für Laserphysik und Zentrum für Optische Quantentechnologien, Universität Hamburg, 22761 Hamburg, Germany. [7]The Hamburg Centre for Ultrafast Imaging, 22761 Hamburg, Germany. [8]Department of Chemistry and Chemical Biology, Harvard University, Cambridge, MA 02138, USA.
*These authors contributed equally to this work.
†Corresponding author. Email: lukin@physics.harvard.edu

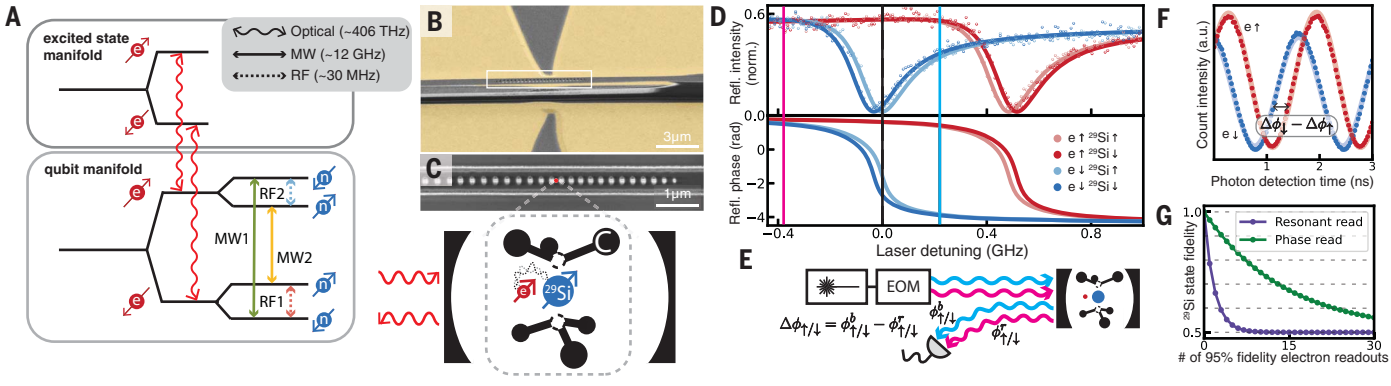

Fig. 1. Quantum network node based on ^{29}SiV. (**A**) Energy-level diagram of the ^{29}SiV. Allowed magnetic dipole transitions are shown by arrows in the qubit manifold for the case when the **B**-field is oriented along the symmetry axis. (**B**) False-color scanning electron microscope (SEM) image of the device, showing the gold coplanar waveguides in yellow. (**C**) Zoomed-in SEM image of the nanophotonic cavity in which the ^{29}SiV is located. (**D**) Spin-dependent reflection intensity (top) and phase (bottom) as a function of laser frequency with a cavity-SiV detuning of $\Delta = 69$ GHz chosen to maximize optical contrast. (**E**) Experimental setup for phase readout of the electron spin state. (**F**) Measured spin-dependent phase shift of the beating pattern between sidebands. (**G**) Coherence of a nuclear superposition state as a function of the number of electron readouts for resonant and phase readouts.

High-fidelity resonant readout of the electron state is achieved by measuring the reflected intensity of a laser at the frequency of maximum reflection intensity contrast (Fig. 1D, black line) (*11*). However, the nuclear qubit experiences dephasing from the laser during readout, with the highest decoherence rate occurring when the laser is near the resonant readout frequency (*21*). To enable selective readout of the electronic spin qubit, we probe the system at laser frequencies at which minimal nuclear dephasing occurs and make use of the electron spin–dependent phase—instead of intensity—of reflected photons for readout. Using an electro-optic modulator (EOM) to generate sidebands (Fig. 1E), we send two tones (blue and magenta lines in Fig. 1D) along the same path and measure the spin-dependent reflected phase difference via the resulting beating pattern to determine the electron state (Fig. 1F) (*21*). With this phase-based readout, the electron can be read 14 times at 95% fidelity before causing a $1/e$ loss of nuclear coherence. This constitutes an eightfold improvement over the resonant readout method (Fig. 1G), with further improvements expected through cavity design and magnetic field optimization (*21*).

The two-qubit ^{29}SiV system is fully controlled by selectively driving the four single-spin–flipping transitions (Fig. 1A) to implement the four possible controlled-NOT (CNOT) gates: two electron-flipping gates C_nNOT_e (MW1) and $\overline{C_nNOT_e}$ (MW2), and two nucleus-flipping gates C_eNOT_n (RF1) and $\overline{C_eNOT_n}$ (RF2), where the absence (presence) of the overbar indicates conditioning on the control spin being in the down (up) state. We measure a fidelity of 99.9 ± 0.1% for the C_nNOT_e gate with a gate time of 30.0 ns. As the time to drive a nuclear π rotation (23 μs) is longer than the electron dephasing time $T_{2,e}^{*}$ (5 μs) (*21*), transfer of electron superposition states onto the nucleus is not possible with direct driving for the C_eNOT_n gate. To circumvent this problem, we increase the electron coherence time using a dynamical decoupling sequence and interleave it with stepwise nuclear rotations (*22*, *23*) to implement a decoupled C_eNOT_n (Fig. 2A). Specifically, we apply RF1 in the first window, and alternate it with applying RF2 after every subsequent unconditional electron π pulse to account for the flipping electron state while keeping the nuclear rotation conditional on the same initial electron state, achieving a gate fidelity of 93.7 ± 0.7% (*21*) within a gate time of 29.2 μs. With the decoupled C_eNOT_n, we can swap a superposition state from the electron onto the nuclear spin state (Fig. 2B), where it can be stored using an XY8 decoupling sequence. We find that the nuclear coherence time scales with n, the number of decoupling pulses applied, as $T_{2,n} \propto n^{0.53}$ with a maximum measured nuclear memory time of $T_{2,n} = 2.1 \pm 0.1$ s (Fig. 2C) when using a 128-XY8 sequence.

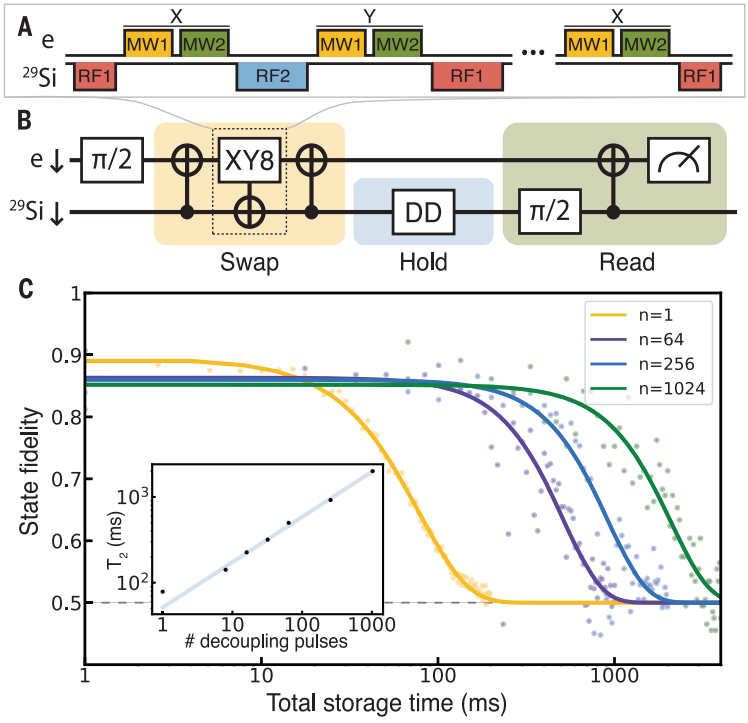

Fig. 2. Long-lived quantum memory based on ^{29}Si nuclear spin. (**A**) Pulse sequence for a decoupled C_eNOT_n gate. (**B**) Sequence for swapping the electron state onto the nucleus, after which a nuclear XY8 decoupling sequence with $n = 1, 64, 256, 1024$ pulses is applied and the nuclear state is measured through resonant readout of the electron. (**C**) Measured nuclear state fidelity after sequence (B). Inset: $T_{2,n}$ as a function of the number of decoupling pulses n fitted to $T_{2,n} \propto n^{\alpha}$ where $\alpha = 0.53$.

To enable robust spin-photon entanglement, we use a SiV with large residual strain [ground state splitting $\Delta_{GS} = 554$ GHz (*21*)], which greatly suppresses the rate of thermal decoherence processes (*19*), enabling operation at 1.5 K without an appreciable reduction in $T_{2,e}$ (Fig. 3A). We implement high-temperature spin-photon entangling gates between the electron spin and time-bin qubits in the $\{|e\rangle, |l\rangle\}$ basis, corresponding to the presence of a photon in either the early or late time bin. The entangling gate sequence (*11*) shown in Fig. 3B generates the entangled state $(|e\downarrow_e\rangle + |l\uparrow_e\rangle)/\sqrt{2}$ conditioned on the detection of a single reflected photon. We find a Bell state fidelity of $F_{e\gamma} = 0.91 \pm 0.02$ (0.90 ± 0.01) at 0.1 K (1.5 K) (Fig. 3C), which is primarily limited by residual reflections from the $|\downarrow_e\rangle$ state and imperfect photonic state measurements.

To further extend the entanglement capabilities of our spin-photon interface, we introduce a photon-nucleus entangling (PHONE) gate that directly entangles the ^{29}Si nuclear spin with a photonic qubit using only fast MW gates and allows operating temperatures up to 4.3 K. In this scheme, the photon-nucleus-electron system is initialized in the $(|e\rangle + |l\rangle)(|\uparrow_n\rangle + |\downarrow_n\rangle)|\downarrow_e\rangle/2$ state, and we apply a sequence of CNOTs as shown in Fig. 3D such that the electron state—and as a result, the SiV reflectivity—in each time bin is conditional on the nuclear state; the final entangled state is given by $(|e\uparrow_n\rangle + |l\downarrow_n\rangle)|\downarrow_e\rangle/\sqrt{2}$. We measure the resulting Bell state fidelity to be $F_{n\gamma} = 0.85 \pm 0.02$ (0.66 ± 0.02) at 0.1 K (4.3 K) (Fig. 3, E and F), with dominant infidelities due to MW gate errors and the nuclear state dependence of the optical transition frequency, which prevents the photon frequency from being tuned to maximize contrast for both nuclear spin states simultaneously (Fig. 1D) (*21*).

A key feature of the PHONE gate is that the electron should always remain in the $|\downarrow_e\rangle$ state after a successful gate application. Because the electron spin mediates the interface between the photon and the nucleus, electron spin flips can be used as an integrated error witness to detect gate errors. Similar to flag qubits in error correction protocols (*24*), PHONE gate errors can be reduced at the cost of some gate failure probability (*25*) by measuring the state of the electron spin qubit (Fig. 4A). Specifically, if the electron spin is measured to be in the $|\uparrow_e\rangle$ state after a PHONE gate application, the prepared photon–nuclear spin entangled state is discarded. As shown in Fig. 4B, the use of the procedure results in a Bell state fidelity increase of 2% (7%) to $F_{n\gamma} = 0.87 \pm 0.02$ (0.71 ± 0.02) with an error detection rate of 8.4% (13.9%) at 0.1 K (4.3 K). In Fig. 4C, we combine all these components to implement a PHONE gate at 4.3 K with error detection and

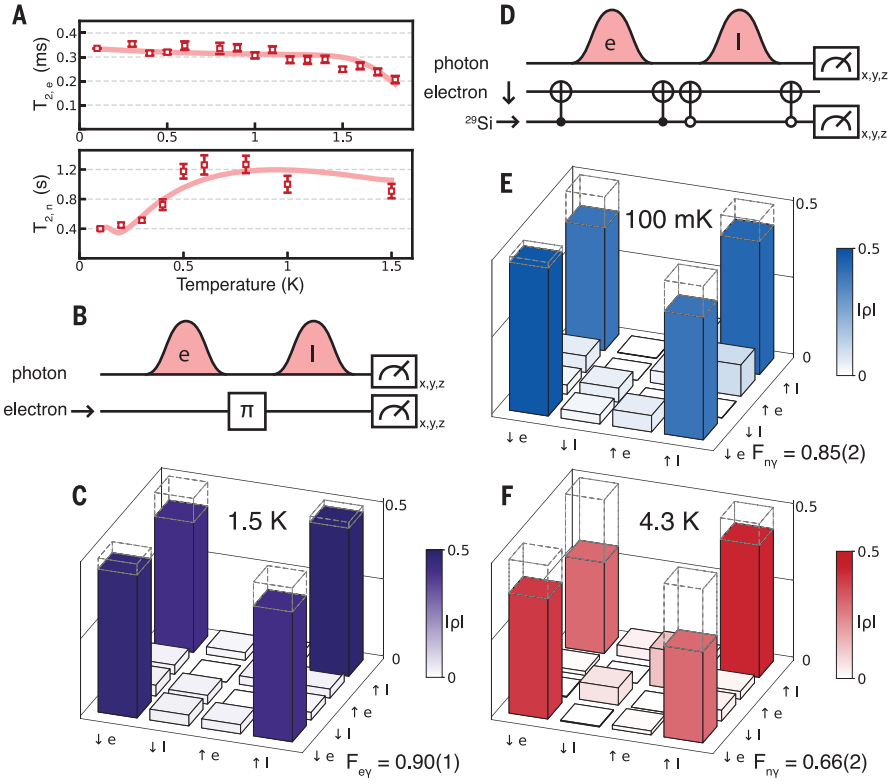

Fig. 3. Spin-photon entanglement at elevated temperatures. (**A**) Coherence time of the electron (top) and nucleus (bottom) obtained using 8-XY8 sequences as a function of temperature. Initial increase of the nuclear $T_{2,n}$ is due to motional averaging of the noise bath. Solid lines are fits to decoherence models of the spin environment described in (*21*). (**B**) Electron spin–photon gate implementation with (**C**) reconstructed density matrix at 1.5 K using resonant electron readout. (**D**) Circuit diagram for the photon-nucleus entangling (PHONE) gate. CNOT gates with black and white control dots refer to C_nNOT_e and $\overline{C_nNOT_e}$ gates, respectively. Reconstructed density matrices for photon-nuclear spin entanglement at (**E**) 100 mK and (**F**) 4.3 K.

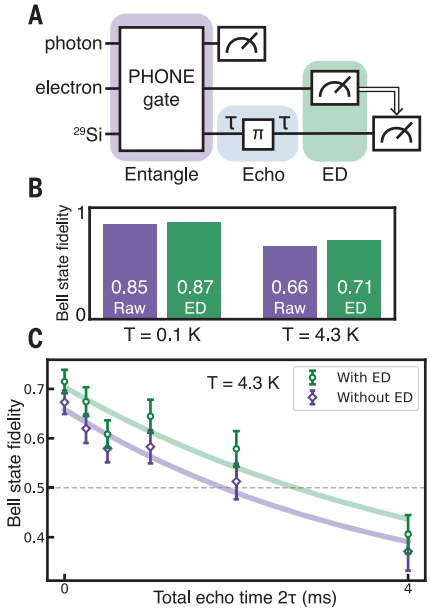

Fig. 4. Spin-photon entanglement with integrated error detection. (**A**) Gate sequence for entanglement between a photon and nucleus and subsequent state storage with error detection (ED) based on resonant readout of the electronic spin. (**B**) Bell state fidelity improvement with ED at 0.1 K and 4.3 K. (**C**) Bell state fidelity as a function of storage time for the sequence shown in (A) before and after error detection. Fits are exponential curves decaying to the maximally mixed-state fidelity $\langle\Phi^+|\rho_{mm}|\Phi^+\rangle = 0.25$ as the nuclear lifetime $T_{1,n}$ is comparable to the coherence time; fitted decay constants are 4.5 (3.8) ms with (without) ED.

store the spin-photon entangled state in the nuclear spin memory using an echo sequence (Fig. 4A) for more than 2.5 ms above the threshold value of 50%, as compared to 1.5 ms without error detection. The error detection protocol detects MW gate errors and $T_{1,e}$- and $T_{2,e}$ -limited depolarization and dephasing, and the large gain in fidelity at 4.3 K is due to the greater contribution of the detectable errors from short $T_{1,e}$ and $T_{2,e}$ times at this temperature (*21*). Conversely, the improvement from error detection at 0.1 K is limited as the infidelity is dominated by nondetectable errors from photon state measurement and SiV optical contrast.

These observations open up several new avenues for realizing quantum networks and exploring their applications. The access to an additional memory qubit directly enables improved memory-enhanced quantum key distribution (*11*) by extending the time window for photons arriving from different communicating parties to the memory node for asynchronous Bell measurement, whereas the phase readout protocol facilitates electron resets between entanglement attempts while information is stored on the nucleus. A nuclear memory can additionally expand the capabilities of the SiV as a single photon source for the creation of photonic cluster states (*26*, *27*). The methods demonstrated here can also enable the deployment of scalable SiV-based quantum repeater networks. Based on a large-scale survey of a second chip fabricated using the current process (*21*), we find that more than 11% of all SiVs are sufficiently strained for operation at 1.5 K, indicating the possibility for a sizable number of highly strained devices in nanophotonic cavities that can operate at elevated temperatures. Moreover, recently demonstrated techniques for strain tuning of nanocavities (*28*) can enable fully deterministic access to high-strain operation. The fidelity gain from our error detection could be larger for more complex spin-photon entangling sequences, such as PHONE-type gates entangling successive photons with the nucleus or entangling a photon with multiple nuclei strongly coupled to the SiV. It also opens opportunities to operate more effectively in regimes where the SiV electron coherence properties deteriorate, including at higher temperatures as demonstrated here, and in a misaligned magnetic field as is required for acoustic spin control (*29*) and single-photon generation (*30*). The use of cavities with higher cooperativity as demonstrated previously (*11*) should allow for higher fidelity and efficiency of electron-spin photon and PHONE gates, as well as improved ^{29}Si state preservation during electron readout (*21*). Finally, nearby ^{13}C spins, such as one associated with the SiV used in this work (*21*), can be used as additional memory resources (*15*, *22*). Apart from realizing multinode quantum network protocols (*8*, *9*), these systems can also allow for the generation of complex photonic tree cluster states that enable robust one-way long-distance quantum communication (*31*).

REFERENCES AND NOTES

1. H. J. Kimble, *Nature* **453**, 1023–1030 (2008).
2. S. Wehner, D. Elkouss, R. Hanson, *Science* **362**, eaam9288 (2018).
3. A. K. Ekert, *Phys. Rev. Lett.* **67**, 661–663 (1991).
4. H.-K. Lo, M. Curty, K. Tamaki, *Nat. Photonics* **8**, 595–604 (2014).
5. E. T. Khabiboulline, J. Borregaard, K. De Greve, M. D. Lukin, *Phys. Rev. Lett.* **123**, 070504 (2019).
6. H. Buhrman, H. Röhrig, *Mathematical Foundations of Computer Science 2003* (Springer Berlin Heidelberg, 2003), pp. 1–20.
7. D. Cuomo, M. Caleffi, A. S. Cacciapuoti, *IET Quantum Commun.* **1**, 3–8 (2020).

8. W. Dür, H.-J. Briegel, J. I. Cirac, P. Zoller, *Phys. Rev. A* **59**, 169–181 (1999).
9. L. Childress, J. M. Taylor, A. S. Sørensen, M. D. Lukin, *Phys. Rev. Lett.* **96**, 070504 (2006).
10. K. Azuma, K. Tamaki, H.-K. Lo, *Nat. Commun.* **6**, 6787 (2015).
11. M. K. Bhaskar *et al*., *Nature* **580**, 60–64 (2020).
12. E. R. Schmidgall *et al*., *Nano Lett.* **18**, 1175–1179 (2018).
13. A. E. Rugar *et al*., *ACS Photonics* **7**, 2356–2361 (2020).
14. X. Guo *et al*., *Nano Lett.* **21**, 10392–10399 (2021).
15. M. Pompili *et al*., *Science* **372**, 259–264 (2021).
16. J. Schupp *et al*., *PRX Quantum* **2**, 020331 (2021).
17. A. Reiserer, N. Kalb, G. Rempe, S. Ritter, *Nature* **508**, 237–240 (2014).
18. K. D. Jahnke *et al*., *New J. Phys.* **17**, 043011 (2015).
19. S. Meesala *et al*., *Phys. Rev. B* **97**, 205444 (2018).
20. B. Pingault *et al*., *Nat. Commun.* **8**, 15579 (2017).
21. Further details on theoretical analysis and additional supporting experimental results are provided in the supplementary materials.
22. C. Bradley *et al*., *Phys. Rev. X* **9**, 031045 (2019).
23. T. van der Sar *et al*., *Nature* **484**, 82–86 (2012).
24. R. Chao, B. W. Reichardt, *Phys. Rev. Lett.* **121**, 050502 (2018).
25. J. Borregaard, P. Kómár, E. M. Kessler, A. S. Sørensen, M. D. Lukin, *Phys. Rev. Lett.* **114**, 110502 (2015).
26. A. Russo, E. Barnes, S. E. Economou, *Phys. Rev. B* **98**, 085303 (2018).
27. C. P. Michaels *et al*., *Quantum* **5**, 565 (2021).
28. B. Machielse *et al*., *Phys. Rev. X* **9**, 031022 (2019).
29. S. Maity *et al*., *Phys. Rev. X* **12**, 011056 (2022).
30. E. N. Knall *et al*., *Phys. Rev. Lett.* **129**, 053603 (2022).
31. J. Borregaard *et al*., *Phys. Rev. X* **10**, 021071 (2020).
32. P.-J. Stas *et al*., Zenodo (2022). https://doi.org/10.5281/zenodo.7101712.

ACKNOWLEDGMENTS

We thank J. Borregaard for discussions and J. MacArthur for assistance with electronics. **Funding:** This work was supported by the NSF, CUA, DoD/ARO DURIP, AFOSR MURI, and DOE (award no. DE-SC0020115). Devices were fabricated at Harvard CNS, NSF award no. 1541959. Y.Q.H. acknowledges support from the A*STAR National Science Scholarship. D.A., E.N.K., and B.M. acknowledge support from an NSF GRFP No. DGE1745303. B.P. acknowledges support through a Marie Skłodowska-Curie fellowship from the European Union's Horizon 2020 research and innovation programme under the Grant Agreement No. 840968 (COHESiV). M.S. acknowledges funding from the NASA Space Technology Graduate Research Fellowship Program. R.R. acknowledges support from the Alexander von Humboldt Foundation and the Cluster of Excellence 'Advanced Imaging of Matter' of the Deutsche Forschungsgemeinschaft (DFG) - EXC 2056 - project ID 390715994. **Author contributions:** P.-J.S., Y.Q.H., B.M., and D.S.L. performed the measurements and analyzed data. B.M. and E.N.K. fabricated the devices. A.S., B.P., M.S., S.D., C.M.K., D.R.A., Y.-C.W., M.B., R.R., and D.S. assisted with experiments. All work was supervised by H.P., M.L., and M.D.L. All authors discussed the results and contributed to the manuscript. **Competing interests:** The authors declare that there are no competing financial interests. **Data and materials availability:** Data and code can be found on Zenodo (*32*).

SUPPLEMENTARY MATERIALS

science.org/doi/10.1126/science.add9771
Supplementary Text
Figs. S1 to S15
Tables S1 to S6
References (*33*–*56*)

Submitted 17 July 2022; accepted 27 September 2022
10.1126/science.add9771

Robust multi-qubit quantum network node with integrated error detection

P.-J. Stas, Y. Q. Huan, B. Machielse, E. N. Knall, A. Suleymanzade, B. Pingault, M. Sutula, S. W. Ding, C. M. Knaut, D. R. Assumpcao, Y.-C. Wei, M. K. Bhaskar, R. Riedinger, D. D. Sukachev, H. Park, M. Lonar, D. S. Levonian, and M. D. Lukin

Science, **378** (6619), .
DOI: 10.1126/science.add9771

A robust quantum network node

The ability to develop quantum networks and communicate quantum information over long distances requires quantum memory nodes with efficient optical interfaces and long memory times. Because of their long coherence times and efficient optical interface, color centers in diamond are promising candidates to achieve this goal. Stas *et al*. use silicon vacancies in diamond and integrated the properties into a single device (see the Perspective by Gangloff). The authors demonstrate a quantum memory with a lifetime exceeding 2 seconds and full optical control of the quantum states of the two-qubit register. With the capability of built-in error detection, such a platform is promising for the development of scalable quantum networks. —ISO